Microcrystallization of Benzene-d_6 in Mesoporous Silica Revealed by ^{2}H Solid-State Nuclear Magnetic Resonance

Wlodzimierz Masierak,[†,‡] Thomas Emmler,[†] Egbert Gedat,[†] Andreas Schreiber,[§] Gerhard H. Findenegg,[§] and Gerd Buntkowsky*[,†]

Institut für Chemie, Freie Universität Berlin, Takustrasse 3, 14195 Berlin, Germany, Department of Biophysics, Medical Academy of Bydgoszcz, ul. Jagiellonska 13, 85-067 Bydgoszcz, Poland, and Stranski-Laboratorium für Physikalische und Theoretische Chemie, Technische Universität Berlin, Strasse des 17, Juni 112, 10623 Berlin, Germany

Received: June 18, 2004; In Final Form: August 16, 2004

Benzene-d_6 confined in a mesoscopically organized, controlled, porous-glass mesocellular foam (MCF), with a pore diameter of 30 nm, is studied by low-temperature solid-state ^{2}H nuclear magnetic resonance (^{2}H NMR) spectroscopy in the temperature range of 90−180 K. The resulting spectra are compared to bulk benzene-d_6 and benzene confined in a mesoporous silica (SBA-15). The comparison shows that the spectra in the MCF are the superposition of an amorphous surface phase and a crystalline inner bulk phase. For the inner crystalline phase, the activation energies coincide with that of bulk benzene. The pore volume and the filling factor indicate that approximately three molecular layers of benzene are present on the inner surfaces.

Introduction

In recent years, novel mesoporous silica materials with ordered arrays of pores of uniform size (periodic mesoporous silica, PMS) or disordered pore geometries have been synthesized.[1−4] PMS materials consist of quasi-crystalline powders, where each crystallite constitutes a large number of more-or-less parallel cylindrical pores. The silica formation occurs in water, using surfactants as structure-directing agents (template). The pore diameters can be adjusted by the templating agents: the diameters are typically 2−4 nm in the case of MCM-41 silicas and 5−12 nm for SBA-15 silicas.[3] Materials with wider pores (up to and greater than 50 nm) but nonperiodic structure can be synthesized by similar procedures. After silica formation, the templating agents are removed by calcination. The high porosity causes a large inner surface of these materials. Because of their wide range of pore sizes, they are very versatile molecular sieves. Because the physical properties of their inner surfaces, such as the surface acidity, can be chemically modified,[5,6] mesoporous silica materials are very promising candidates for catalytic applications, which has triggered several recent studies of the dynamics of guest molecules in mesoporous silica.[7−14]

The pores can accommodate small guest molecules, either as individual (gaslike) species or as a condensed phase, interacting with the pore surfaces. The solid−fluid interaction at the pore walls causes a perturbation of the three-dimensional ordering and will thus affect the freezing of the guest phase in the pores. Specifically, the molecules in the direct vicinity of the surface experience forces, according to the surface material and geometry, that generally are not compatible with the crystal packing forces of the crystal lattice.[15] As a result, the molecules in the vicinity of the surface will not easily align in the proper crystal positions and the formation of a crystal lattice is hindered or prohibited near the surface, leading to the formation of amorphous or ordered liquid phases, similar to those in liquid crystals. In the vicinity of the surface, there will be vacancies and structural defects, which can enhance translational diffusion of the guest molecules and molecules in this surface phase will generally exhibit an increased rotational mobility at lower temperatures, as compared to the molecules in the crystalline phases. The dynamic behavior of molecules in this surface phase is expected to be dominated by the solid−liquid interaction. For large pore diameters, an additional inner pore volume phase can form, which is expected to have properties similar to those of the bulk phase. Note that such features are quite common, for example, in aqueous protein solutions, where a layer of nonfreezable water in the hydration shell of the protein coexists with a phase of freezable bulk water.[16−22]

In a recent publication, the rotational dynamics of benzene-d_6 in the mesopores of SBA-15 have been studied, employing solid-state ^{2}H NMR spectroscopy in the temperature regime of 19−240 K. In this study, evidence was found for the existence of a strongly disordered, glasslike benzene phase inside the mesopores. This glasslike phase was characterized by a very broad distribution of correlation times for the rotational degrees of freedom (6-fold rotation around the molecular C6 axis, or isotropic reorientations of the C6 axis). Because such broad distributions are typically found in glassy systems,[23−26] we termed it a "glasslike" surface phase. From the pore volume and the filling factor of the pores, a thickness of ca. four molecular layers of this surface phase was estimated. This observation provokes the question of how many molecular layers are required to change from a surface-induced disordered phase to an ordered (i.e., crystalline) inner phase with a disordered boundary layer. To answer this question, we studied benzene in a mesoporous silica material, prepared in a manner similar

* Author to whom correspondence should be addressed. Present address: Friedrich Schiller Universität Jena, Institut für Physikalische Chemie, Helmholtzweg 4, D-07743 Jena. E-mail: gerd.buntkowsky@uni-jena.de. Telephone: +49 3641 948310. Fax: +49 3641 948302.

[†] Freie Universität Berlin.
[‡] Medical Academy of Bydgoszcz.
[§] Technische Universität Berlin.

10.1021/jp047348r CCC: $27.50
Published on Web 11/12/2004

to that for SBA-15, but having significantly larger pores (ca. 30 nm), with a pore morphology resembling that of a mesocellular foam (MCF).[27−29]

Before going into the details of our study, we briefly summarize some salient factors about the influence of the rotational states of benzene on its solid-state ^{2}H NMR spectrum.[30−32] If the correlation times of the different rotational motions are on the time scale of that for ^{2}H NMR, the mobility of benzene-d_6 can be directly monitored by ^{2}H NMR line shape analysis. The line shapes of the ^{2}H NMR spectra reveal the motional averaging of the quadrupolar coupling tensor,[33,34] which acts as a sensor for the state of ordering of the benzene. In bulk benzene, three states of different rotational freedom can be distinguished by ^{2}H NMR, namely, a liquid state and two solid states: The first (liquidlike) state corresponds to fast isotropic rotational motions of the benzene molecule, whereas the second state (solid I) is an anisotropic rotational jump diffusion around the 6-fold axis and the third state (solid II) is the fully frozen state, where no rotational motion is present. In the region of the solid I−solid II transition, where the rate of the 60° jump is comparable to quadrupolar frequencies, typical motion-induced deviations from the common Pake pattern line shape are observed. These line shapes were reported by Vold et al.[30] for bulk benzene-d_6 and for benzene-d_6 confined in the cages of the cyclamer 1,3-cyclohexanedione. From the properties of bulk benzene, it is expected that the fully frozen (solid II) state will also prevail in silica pores at temperatures well below 100 K. For glasslike systems of benzene, however, a different behavior has been observed.[31] Here, a broad distribution of correlation times of the 6-fold jump motion renders the spectra corresponding to the intermediate motional range of the solid I−solid II transition invisible. This leads to spectra that are a weighted superposition of molecules rotating slowly on the NMR time scale with solid-II-like spectra and molecules rotating fast on the NMR scale with solid-I-like spectra. We obtained a similar result in the benzene-d_6 system in SBA-15, as discussed previously.

The rest of the paper is organized as follows: First, the experimental section gives a short introduction into the basics of ^{2}H NMR line shape theory and describes the synthesis of the mesoporous silica materials, the NMR sample preparation, and our low-temperature ^{2}H NMR setup. The characterization of the material via X-ray diffraction and gas adsorption, and the results of the experimental low-temperature ^{2}H NMR study of bulk benzene-d_6, and benzene-d_6 as guest molecule in the mesoporous silica MCF then are presented, discussed, and finally summarized.

Experimental Section

^{2}H Nuclear Magnetic Resonance Powder Spectra. The basic theory of solid-state ^{2}H NMR is well-known[35,36] and only briefly summarized here. The leading interaction in solid-state ^{2}H NMR is the ^{2}H quadrupolar interaction. In the usual high-field approximation, the first-order quadrupolar interaction is characterized by the Hamiltonian

$$\hat{H}_Q = 2\pi\nu_Q(\vartheta,\varphi)\left(\hat{I}_z^{\,2} - \frac{2}{3}\right) \tag{1}$$

where the orientation-dependent resonance frequencies ν_Q of the two transitions are given as

$$\begin{aligned}\nu_Q(\vartheta,\varphi) &= \pm\frac{3}{4}\left(\frac{eQeq}{\hbar}\right)\frac{1}{2}(3\cos^2\vartheta - 1 - \eta\sin^2\vartheta\cos 2\varphi) \\ &= Q_{zz}\frac{1}{2}(3\cos^2\vartheta - 1 - \eta\sin^2\vartheta\cos 2\varphi)\end{aligned} \tag{2}$$

where η is an asymmetry parameter and Q_{zz} is the strength of the quadrupolar interaction. Although, in single crystals, only two lines at $\pm\nu_Q$ are observable, the average over all possible orientations must be calculated in a nonoriented powder sample. Because of the axial symmetry of the magnetic field, it is sufficient to integrate over two angles (ϑ, φ) only. Assuming, for simplicity, that the transversal relaxation time T_2 is independent of orientation, the spectra can be calculated as a superposition of the lines with the line shape function $f(\nu,\pm\nu_Q,T_2)$ of the individual crystallites:

$$I(\nu) = \int_0^{\pi} d\vartheta \sin(\vartheta)\int_0^{2\pi} d\varphi\,(f(\nu,-\nu_Q(\vartheta,\varphi),T_2) + f(\nu,+\nu_Q(\vartheta,\varphi),T_2)) \tag{3}$$

The quadrupolar coupling constant $Q_{cc} = (^4/_3)Q_{zz}$ is a measure of the strength of the quadrupolar interaction. For rigid benzene (solid II state), a practically axial symmetric quadrupolar tensor with $\eta < 0.05$ and a value of $Q_{zz} \cong 140$ kHz is observed. Because of the large spectral width, the ^{2}H NMR spectra are measured with the solid echo sequence $[90^\circ_y - \tau - 90^\circ_x - \tau - \langle\hat{I}_x\rangle]$. If the molecule undergoes fast reorientations, the value of the quadrupolar tensor and, thus, also the quadrupolar coupling in general are changed, depending on the type and speed of the motion.[33] If the motions are fast on the NMR time scale, a relatively simple scenario is found: fast isotropic reorientations of the benzene molecule (as, for example, that in liquid benzene) cause a complete averaging of the quadrupolar tensor ($Q_{zz}^{iso} = 0$). Anisotropic rotations or rotational jump diffusions around the C_6-axis reduce the value of Q_{zz} to $Q_{zz}^{rot} = (^1/_2)Q_{zz}$. In these situations, the normalized line shape of the solid echo spectrum is identical to the Free Induction Decay (FID) spectrum.

This is no longer the case if the correlation time of the motion is on the NMR time scale. Here, the situation is more complicated, in particular, if a distribution of rotational correlation times for the motion exist. Two limiting cases must be considered, namely (a) if the distribution function is very narrow (crystalline behavior) and (b) if the distribution function is very broad (glasslike behavior). In the case of a crystalline behavior, the line shape of the solid echo spectra is dependent very strongly on the echo delay time τ and the rotational correlation time.[30] The line shape of the solid echo spectra must be calculated using standard NMR methods.[36] In the glasslike case, however, the spectra are always simple superpositions of the slow and fast limit spectra with varying weights.

Synthesis and Characterization of the Mesoporous Silica. A mesoporous silica designated as MCF was synthesized by a process similar to that used for the preparation of SBA-15,[3] using a PEO−PPO−PEO triblock copolymer (Pluronic P123) as the structure directing agent, but with the addition of an equal mass of 1,3,5-trimethylbenzene to the aqueous reaction mixture, to boost the pore size. Details of the synthesis of this sample are given elsewhere.[37] Transmission electron microscopy (TEM) images of the calcined samples (Figure 1) indicate that the pore structure of this material is grossly different from that of SBA-15. Pores of approximately circular cross section with a diameter of ca. 30 nm are arranged in a disordered manner, similar to the mesocellular siliceous foams reported by Schmidt-Winkel and co-workers.[27−29]

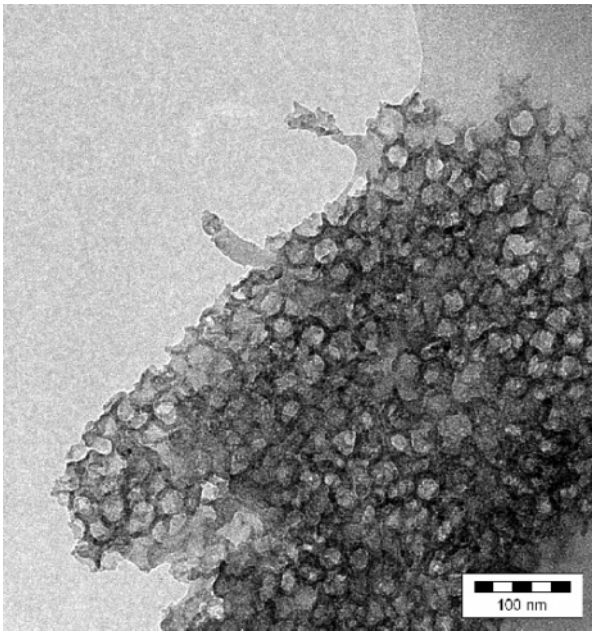

Figure 1. Transmission electron microscopy (TEM) micrograph of an ultramicrotomed mesocellular foam (MCF) sample, showing the pore morphology of the material. Scale bar represents 100 nm.

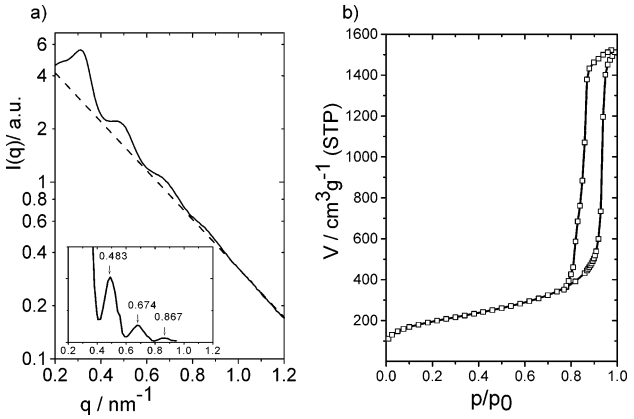

Figure 2. Characterization of the MCF sample: (a) small-angle powder X-ray diffraction curve (inset shows a magnified view of the three local maxima of $I(q)$ at $q > 0.4$ cm^{-1} after subtraction of a background term, as indicated by the dashed line); (b) nitrogen adsorption isotherm (at 77 K) with the pore condensation step and H1 type hysteresis loop (the full line is a guide to the eye).

The structure of the sample was characterized by small-angle X-ray scattering (SAXS), using a Kratky compact camera. The scattering curve $I(q)$, which is shown in Figure 2a (where q is the scattering vector ($q = (4\pi/\lambda) \sin \theta$)), exhibits a pronounced peak at $q = 0.31$ nm^{-1} and three equidistant local maxima separated by $\Delta q = 0.192$ nm^{-1}. The first peak represents a structure peak resulting from the packing of the pores. The maxima and minima at higher q values, which are much broader than typical Bragg peaks, are attributed to the form factor of the pores. The form factor of a sphere of radius R exhibits a series of sharp minima at q values corresponding to the condition $qR = 3\pi/2, 5\pi/2, 7\pi/2, ...$; thus, from the distance between neighboring minima (or maxima) in the scattering curve, the radius of the spheres can be derived as $R = \pi/\Delta q = 16.3$ nm. The fact that three maxima of the form factor can be resolved (see inset in Figure 2a) is strong evidence that the pores in MCF silica have a rather uniform size (otherwise, the minima in $I(q)$ would be blurred by the polydispersity). On the other hand, the scattering curve provides no proof that the pores have a spherical shape, because the form factor of a cylinder also exhibits equidistant minima separated by $\Delta q = \pi/R$, where R is now the radius of the cylinder. The absence of Bragg peaks in the scattering curves implies that MCF has a disordered pore structure. Most likely, it constitutes a random packing of spherical pores of almost uniform size, because it is difficult to imagine an irregular packing of cylindrical pores of uniform size in a matrix of high porosity, as for the present material.

TABLE 1: Characterization of the Mesocellular Foam (MCF) Silica by Nitrogen Adsorption (at 77 K)

property	value
BET specific surface area, a_s[a]	674 m^2/g
specific pore volume, υ_p	2.34 cm^3/g
porosity, ϵ	0.834
BJH mean pore diameter[b]	
D_{ads}	33.1 nm
D_{des}	15.0 nm

[a] Determined using Brunauer−Emmett−Teller methodology (see ref 39). [b] Determined using Barrett−Joyner−Halenda methodology (see ref 40).

The porosity of the MCF material was characterized by nitrogen adsorption, using a Micromeritics model Gemini 2375 volumetric gas adsorption analyzer. The nitrogen adsorption isotherm of a sample, outgassed at 110 °C and 10^{-4} Torr, is shown in Figure 2b. The isotherm exhibits an almost vertical pore condensation step and an almost equally steep pore evaporation step (H1-type hysteresis loop), which is indicative for pores of uniform size and shape. The specific surface area a_s (derived by the BET method), the specific pore volume υ_p and porosity ϵ, and the mean pore diameter D are summarized in Table 1. The value of υ_p was determined from the amount of nitrogen adsorbed at a relative pressure of $p/p_0 = 0.995$, and the porosity $\epsilon = \rho_s\upsilon_p/(1 + \rho_s\upsilon_p)$ was derived from υ_p, using a skeleton density of $\rho_s = 2.15$ g/cm^3, as determined for SBA-15 materials by helium displacement.[37] The mean pore diameter D was evaluated from the pore condensation and pore evaporation pressures ($(p/p_0)_{ads} = 0.937$ and $(p/p_0)_{des} = 0.855$, where p_0 is the saturated vapor pressure at the experimental temperature), on the basis of the Dollimore and Heal[38] prescription for the thickness of the physisorbed nitrogen film.[37,38] The value of the pore diameter derived from the adsorption branch ($D = 33$ nm) is in very good agreement with the value derived from the analysis of the small-angle X-ray scattering (SAXS) curve.

Nuclear Magnetic Resonance Samples. A sample of MCF silica loaded with benzene-d_6 was prepared by placing 17.4 mg of MCF into a standard 5-mm NMR tube and outgassing at 160 °C at 10^{-4} mbar for 2 h to remove any moisture and gases from the pores and clean the inner surfaces. Afterwards, the dry sample was weighed (14.3 mg) and, from the specific pore volume υ_p, the total pore volume of this sample was estimated to be 33.5 μL. A liquid volume of 26.8 μL (25.4 mg) of benzene-d_6 99.6% (Aldrich) was then added to the silica, corresponding to a nominal degree of filling of only 80% of the pore space, to make sure that all benzene is indeed contained in the pore space and no extra benzene is found outside the pores.

Low-Temperature ^{2}H Nuclear Magnetic Resonance. A detailed discussion of our home-built three-channel NMR spectrometer has been given recently.[41,42] Here, only some salient features are reproduced. All experiments were performed at a field strength of 6.98 T, corresponding to a ^{2}H resonance frequency of 45.7 MHz on a standard Oxford wide-bore magnet (89 mm) equipped with a room-temperature shim unit. For the ^{2}H-channel, a 2 kW class AB amplifier (from AMT) equipped with an RF-blanking for suppressing the noise during data

acquisition was used. The RF was fed through a crossed diode duplexer, which was connected to the detection preamplifier and through the filters into the probe. Typical ^{2}H pulse width was 5.0 μs, corresponding to 50 kHz B_1-field in frequency units. To achieve a better excitation of the echo spectrum, a shortened pulse width of 3.50 μs was used.

All experiments were performed using a home-built 5-mm ^{2}H NMR probe. The probe is placed in a dynamic Oxford model CF1200 helium flow cryostat. The sample temperature was controlled using an Oxford ITC 503 temperature controller. During cooling and before and after data acquisition, the sample temperature was directly controlled via a Cernox sensor that was placed in the direct vicinity of the sample. This temperature was used to calibrate the readings of a second CGR-1-1000 sensor, which is part of the cryostat. During data acquisition, the first sensor was disconnected from the ITC 503 temperature controller and grounded to protect the controller from the RF and avoid distortions of the signal. Because of the high sensitivity of the ^{2}H NMR line shapes of both bulk and guest benzene-d_6 on the temperature, we carefully monitored the stabilization and equilibration of the temperature, allowing stabilization times up to several hours at each temperature before performing the NMR experiment.

All spectra were recorded in resonance using the solid echo technique, with an echo spacing of 30 μs and a full 32-step phase cycle, which removes artifacts from FIDs of the two pulses. Before Fourier transformation, the echo signal was phase-corrected and the imaginary part zeroed to give fully symmetric spectra, which are better suited for the line shape analysis. For the measurements of the benzene guests in the silica pores, we had to ensure that the complete magnetization of all benzene molecules was fully relaxed and a quantitative evaluation of the concentrations of the molecules in the different rotational states is possible (see below). Therefore, several test spectra with different recycle delays were measured at each temperature. From these tests, the optimal recycle time was determined, which was used for measuring the final spectrum. Recycle delays varied between 3 s (high temperature) and 120 s (lowest temperature). For the interpretation of the ^{2}H NMR solid echo spectra of benzene-d_6 in the pores of SBA-15, the temperature-dependent spectra of the bulk benzene in the solid state are necessary as reference. Here, we use the spectra that we published in a recent paper[43] (see Figure 3).

Data Evaluation. The echo spectra of benzene-d_6 in the fast and slow exchange regimes were simulated using eq 3, using a laboratory-written Matlab program. Instead of numerically performing the powder integration, the faster analytical expression of the powder pattern, in terms of elliptic integrals,[44] was used to calculate the line shape for infinite T_2. The ^{2}H NMR echo spectra of the benzene in the intermediate exchange regime were simulated by a self-written Matlab routine, using a Liouville formalism of the exchange process. For the powder integration over the polar angles (eq 3), optimized angle sets with 556 and 16574 angles were used.[45−47] The simulation program was tested by reproducing the calculations shown in ref 30. Effects of the finite pulse power were taken into account using the formula given in ref 36. Because the width of the spectra is much larger than the natural line width of the individual crystallites, a simple Lorentzian was chosen as the line shape function $f(\nu,\pm\nu_Q,T_2)$ in eq 3. The resulting Pake spectra were numerically convoluted with this Lorentzian by Fourier transformation into the time domain, multiplication with a decaying exponential function, and transformation back into the frequency domain. In the MCF sample, where two different sub-spectra are present (see results), the relative intensities of different spectral contributions were calculated from the integrals over the lines of the corresponding sub-spectra.

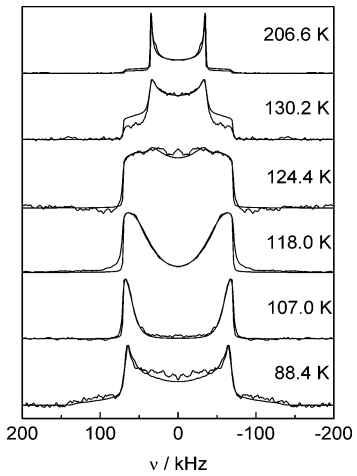

Figure 3. ^{2}H NMR spectra (solid line) and solid echo simulations (broken line) of bulk benzene-d_6 at various temperatures (taken from ref 43). In the temperature range of the transition from the solid I state (206.6 K) with a narrow Pake pattern ($Q_{zz} \cong 70$ kHz) to the solid II state (88.4 K) with a broad Pake pattern ($Q_{zz} \cong 140$ kHz), the rotational jump around the 6-fold axis causes strong deviations from the Pake line shape.

Results and Discussion

^{2}H Nuclear Magnetic Resonance Spectra of Bulk Benzene. As discussed previously for the interpretation of the complex ^{2}H NMR spectra of benzene in MCF, knowledge of the spectra of bulk benzene, as a function of the temperature, is essential.

For this purpose, Figure 3 reproduces the superposition of the experimental and simulated ^{2}H NMR spectra of bulk benzene in the temperature range between 206.6 and 88.4 K from ref 43. The high-temperature spectrum at 206.6 K shows the solid I spectrum of bulk benzene-d_6 with a strength of the quadrupolar interaction of $Q_{zz}^{rot} = Q_{zz}/2 = 67.75$ kHz. It represents the fast jump limit (high-temperature limit). In the temperature region between 130.2 and 107.0 K, the jump rate is comparable to the NMR time scale and the typical effects on the line shape of the solid echo spectra[48] are visible, as discussed by Vold et al. for benzene-d_6.[30] At 88.4 K, the slow jump limit (low-temperature limit) is reached with the solid II spectrum with $Q_{zz} = 133$ kHz. From the simulation of the data, the rate constants of the 60° jumps around the molecular axis, as a function of the inverse temperature, are determined.

The data (open squares in Figure 4) exhibit a typical thermally activated Arrhenius-type behavior ($k = k_0 \exp[E_a/(RT)]$). From the corresponding fit, a pre-exponential factor of $k_0 = 2.0 \times 10^{13}$ s^{-1} and an activation energy of $E_a = 16.8$ kJ/mol are determined.

^{2}H Nuclear Magnetic Resonance Spectra of Benzene in Mesocellular Foam (MCF). From the bulk-benzene experiments, it is evident that a crystalline benzene phase with similar properties is expected to have fairly long T_1 relaxation times at temperatures <90 K and will have the rotational phase transition from the solid I state to the solid II state at temperatures of 100−130 K. Only this phase transition allows the distinction of a crystalline phase from an amorphous, glasslike surface phase; therefore, the spectra measured in this temperature range should allow distinction between the different phases.

Figure 5 displays the experimental ^{2}H NMR spectra of benzene-d_6 confined in the pores of the mesoporous silica MCF

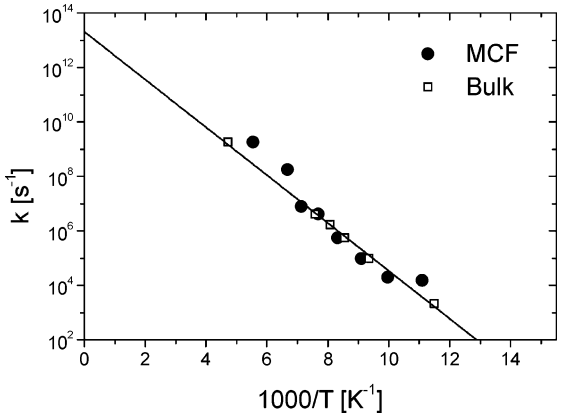

Figure 4. Arrhenius fit of the temperature-dependent jump rates of bulk benzene-d_6 (from ref 43) and of the crystalline core phase (new data, see below). In both cases, the fit yields an activation energy of $E_a = 16.8$ kJ/mol and a pre-exponential factor of $k_0 = 2.0 \times 10^{13}$ s^{-1}, showing that the crystalline core phase is indeed a crystalline benzene phase.

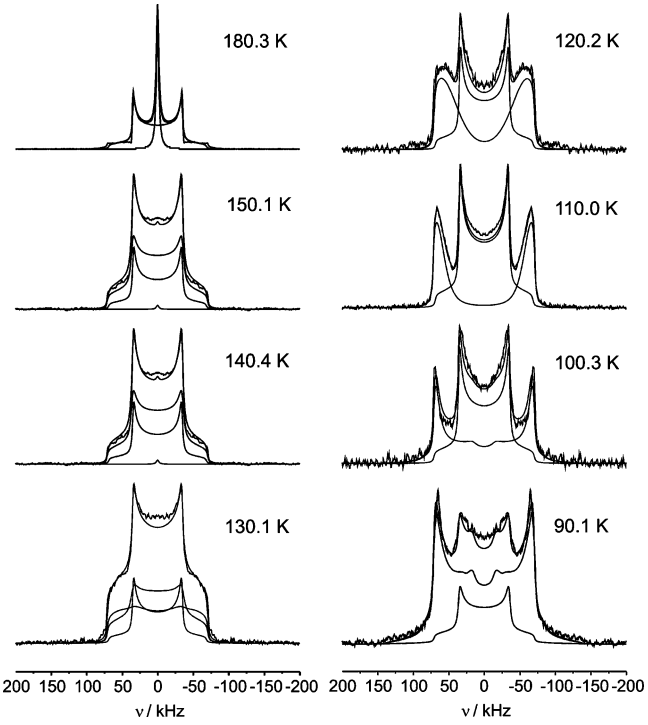

Figure 5. ^{2}H NMR spectra and simulations of benzene-d_6 confined in the pores of the mesoporous silica MCF for various temperatures. In the temperature regime of 110−130 K, the spectra clearly consists of sub-spectra from crystalline benzene and glasslike benzene.

in the temperature range of 90.1−180.3 K. At all temperatures, the spectra exhibit a fairly complex line shape. Each spectrum represents a superposition of several lines with varying intensity ratio. A simulation of these spectra as a pure amorphous benzene phase, characterized by a simple superposition of solid I and solid II components with varying intensity ratios, leads to no satisfactory represention of the experimental line shape, in particular for the spectra measured at 110 and 120 K (simulation not shown). Closer inspection reveals that the outer part of these spectra strongly resembles the bulk benzene spectra measured at 118 and 124 K. This is already a strong indication of a well-ordered, bulklike crystalline benzene phase in the pores, which exists in addition to the disordered inner surface phase. To corroborate the interpretation of these line shapes, we performed a full line shape analysis of all spectra. In this analysis, the

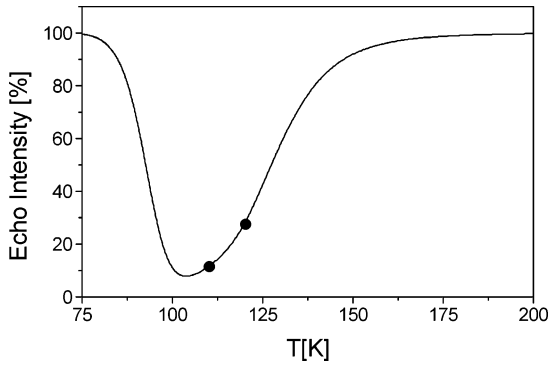

Figure 6. Calculated solid-echo intensity as a function of temperature; the black circles mark the attenuations that were used to determine the volume of the inner crystalline phase.

spectra were simulated as a superposition of four different spectral components—namely, the three different states (liquid, solid I, and solid II), plus a bulklike crystalline line with well-defined rotational correlation time for the 6-fold jump. The resulting simulations (also shown in Figure 5) are in excellent agreement with the experimental line shape, showing that, indeed, such a bulklike crystalline phase exists inside the pores.

Discussion. From the experimental spectra, it is evident that a bulklike crystalline phase and a disordered glasslike phase coexist in the pores of MCF. Because the surface will have a strong disordering effect on the benzene molecules, it is safe to assume that the disordered glasslike phase is located at the surface and the ordered bulklike crystalline phase is, accordingly, in the center of the pores. This result now raises two questions, namely

(1) What is the relative size of the two phases, in terms of molecular layers?

(2) How does the bulklike crystalline core phase compare to a pure bulk phase?

The first question can be answered from the relative number of molecules in the two phases (N_{Core}, N_{Glass}), which is accessible by the relative intensities of the spectral components (I_{Core}, I_{Glass}). As discussed previously in the materials section, the pore structure of MCF is less regular than the structure of SBA and consists of interconnected monodisperse spherical pores. Because of the interconnection of the pores, there is no confinement and the benzene molecules can, in principle, move freely through the MCF. Because it is relatively difficult to model this structure, we consider two simple model cases, namely, a model of concentric cylinders and a model of concentric spheres, which are the mathematical limits for the interconnected sphere structure. For both models, the number of molecules can be determined by simple geometric arguments (see Appendix).

For a quantitative evaluation, the following two points must be considered: (i) the crystalline bulklike phase must be clearly distinguishable from slow molecules in the glasslike phase, and (ii) the effects of the echo attenuation due to the molecular motion must be included into the quantitative evaluation. The best separation between the phases is given for the spectra measured at 110 and 120 K, where all molecules of the bulklike core phase constitute the broad component and those of the glasslike phase constitute the narrow component.

From the echo attenuation curve (Figure 6), correction factors of 11.4% and 27.5% are obtained at 110 and 120 K, respectively. Using these factors, the corrected relative intensities of the phases (see Appendix) are I_{Core}:I_{Glass} = 0.82:0.18 at 110 K and I_{Core}:I_{Glass} = 0.79:0.21 at 120 K. A second independent measure of the relative ratio is obtained from the high-temperature

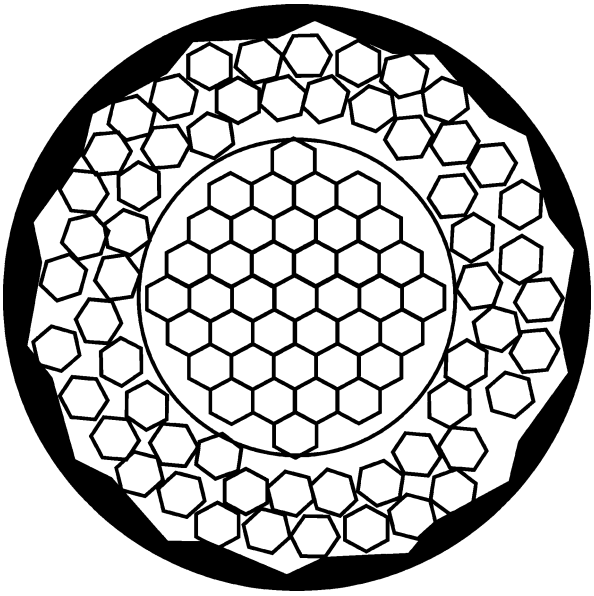

Figure 7. Sketch of the benzene phases inside MCF (not to scale). An inner crystalline core phase is present, as well as an outer amorphous surface phase. The latter has an average thickness of 2−3 molecular layers. The circle symbolizes a hypothetical boundary between the two phases.

spectrum measured at 180 K. Here, the liquidlike central line corresponds to benzene molecules in the glasslike surface phase and the solid line corresponds to the core phase. The relative intensity ratios are I_{Core}:I_{Glass} = 0.77:0.23 at 180 K. All three values coincide, within the experimental error. From these data, the calculated molecular thickness of the surface phase is 1.5 nm (at 110 K) and 1.8 nm (at 120 K) for the cylinder model and 1.0 nm (at 110 K) and 1.2 nm (at 120 K) for the spherical model. Taking the average of the values at temperatures of 110 and 120 K, we find that $d = 1.65 \pm 0.2$ nm for the cylindrical and $d = 1.1 \pm 0.2$ nm for the spherical model. These values can be compared to typical benzene distances in the solid. Using the X-ray data of bulk benzene (space group *Pbca*, $a = 0.7460$ nm, $b = 0.9666$ nm, and $c = 0.7034$ nm, four molecules per unit cell),[49] a typical next-neighbor distance of 0.5 nm for bulk benzene is calculated. Assuming that the density in the inner surface phase is approximately the same as that in bulk benzene, it follows that the surface phase has an average thickness of ∼2−3 molecular layers of benzene. This value is in good agreement with our estimates in the previous study,[43] where we proposed a thickness of four molecular layers of benzene. Part of the one-molecule difference might be attributed to the considerable surface roughness of SBA-15, which is caused by $(SiO_2)_n$ islands on the pore surface.[50,51]For the second question, it is necessary to characterize the hindering potentials of the benzene molecule in the crystalline core phase and compare it to the pure bulk benzene. This hindering potential can be described by the activation energy of the 60° jumps around the molecular axis. For determination of the activation energy, the rate constants of the 60° jumps around the molecular axis are determined from the simulation of the core components and plotted in an Arrhenius diagram as a function of the inverse temperature (filled circles in Figure 4). Comparing these data with the data of the pure bulk benzene, it is evident that the rate constants belonging to the temperatures of 100−140 K are in excellent agreement with the bulk data. At temperatures above 140 K and below 100 K, there are some small deviations between the data of the pure bulk phase and the data of the crystalline core phase. These deviations are mainly an experimental artifact, because the line shape at temperatures similar to that for the solid I or solid II limit (i.e., low temperatures or high temperatures) is relatively insensitive, in regard to temperature. Accordingly, these data points must be neglected for the determination of the activation energy and pre-exponential factor of the Arrhenius law. Thus, the crystalline core phase is characterized by the same activation energy and pre-exponential factor as the pure bulk phase, i.e., a pre-exponential factor of $k_0 = 2.0 \times 10^{13}$ s^{-1} and an activation energy of $E_a = 16.8$ kJ/mol.

Summary and Conclusion

By careful selection of the pore diameter and preparation of the sample, we were able to prepare a superposition of an inner surface and an inner bulk phase of benzene molecules as guests in the mesopores of the controlled porous glass mesocellular foam (MCF) with a pore diameter of 30 nm. In the inner bulk phase, there is a relatively narrow transition temperature distribution for the rotational motion ("six-fold hopping") of the benzene molecules around their molecular symmetry axis. The activation energy of the hopping coincides with the value of bulk benzene. Thus, the inner bulk phase can be identified as a crystalline phase of benzene. The benzene molecules in the inner surface phase exhibit a glasslike, broad distribution of rotational correlation times for the 6-fold jump of the benzene molecules. From the relative intensity of the two phases, the thickness of the amorphous surface layer can be estimated to be ca. three molecules.

In conclusion, it has been shown that ^{2}H NMR is a valuable tool for the characterization of surface processes in mesoscopically organized solids, which allows for a quantitative estimation of the number of molecular layers over which the influence of the surface is transmitted.

Acknowledgment. This work was supported by the Deutsche Forschungsgemeinschaft in the framework of the Sonderforschungsbereich 448 "Mesoskopisch Strukturierte Verbundsysteme". W.M. acknowledges a one-year fellowship of the European Union in the Marie-Curie Program (under Contract No. HPMT-CT-2000-00127). This work is dedicated to the memory of our friend and mentor, Prof. Dr. Aleksander Gutsze.

Appendix

For the two limiting cases of pore structure, the relative amounts of surface and inner bulk molecules are determined by simple geometric arguments.

Cylindrical Pores. In the case of cylindrical pores, the relative amount of the two types of molecules is

$$\frac{N_{Core}}{N_{Glass}} = \frac{V_{Core}}{V_{Glass}} = \frac{\pi h R_{Core}^2}{\pi h (R_{Pore}^2 - R_{Core}^2)} = \frac{R_{Core}^2}{R_{Pore}^2 - R_{Core}^2} \quad \text{(A1)}$$

From this relation, the radius of the inner bulk phase is determined as

$$R_{Core} = R_{Pore}\sqrt{\frac{N_{Core}}{N_{Glass} + N_{Core}}} = R_{Pore}\sqrt{\frac{I_{Core}}{I_{Glass} + I_{Core}}} \quad \text{(A2)}$$

The thickness of the surface phase (d) is given by

$$d = R_{Pore} - R_{Core} = R_{Pore}\left(1 - \sqrt{\frac{I_{Core}}{I_{Glass} + I_{Core}}}\right) \quad \text{(A3)}$$

Spherical Pores. In the case of spherical pores, the relative amount of the two types of molecules is

$$\frac{N_{\mathrm{Core}}}{N_{\mathrm{Glass}}} = \frac{V_{\mathrm{Core}}}{V_{\mathrm{Glass}}} = \frac{(4/3)\pi R_{\mathrm{Core}}^3}{(4/3)\pi(R_{\mathrm{Pore}}^3 - R_{\mathrm{Core}}^3)} = \frac{R_{\mathrm{Core}}^3}{(R_{\mathrm{Pore}}^3 - R_{\mathrm{Core}}^3)} \tag{A4}$$

From this relation, the radius of the inner bulk phase is determined as

$$R_{\mathrm{Bulk}} = R_{\mathrm{Pore}}\sqrt[3]{\frac{N_{\mathrm{Core}}}{N_{\mathrm{Glass}} + N_{\mathrm{Core}}}} = R_{\mathrm{Pore}}\sqrt[3]{\frac{I_{\mathrm{Core}}}{I_{\mathrm{Glass}} + I_{\mathrm{Core}}}} \tag{A5}$$

The thickness of the surface phase d is given by

$$d = R_{\mathrm{Pore}} - R_{\mathrm{Core}} = R_{\mathrm{Pore}}\left(1 - \sqrt[3]{\frac{I_{\mathrm{Core}}}{I_{\mathrm{Glass}} + I_{\mathrm{Core}}}}\right) \tag{A6}$$

References and Notes

(1) Linssen, T.; Cassiers, K.; Cool, P.; Vansant, E. F. *Adv. Colloid Interface Sci.* **2003**, *103*, 121.
(2) Selvam, P.; Bhatia, S. K.; Sonwane, C. G. *Ind. Eng. Chem. Res.* **2001**, *40*, 3237.
(3) Schreiber, A.; Ketelsen, I.; Findenegg, G. H. *Phys. Chem. Chem. Phys.* **2001**, *3*, 1185.
(4) Schüth, F.; Schmidt, W. *Adv. Eng. Mater.* **2002**, *4*, 269.
(5) Anwander, R.; Nagl, I.; Widenmayer, M.; Engelhardt, G.; Groeger, O.; Palm, C.; Röser, T. *J. Phys. Chem. B* **2000**, *104*, 3532.
(6) Whilton, N. T.; Berton, B.; Bronstein, L.; Hentze, H.-P.; Antonietti, M. *Adv. Mater.* **1999**, *11*, 1014.
(7) Hansen, E. W.; Schmidt, R.; Stöcker, M.; Akporiaye, D. *Microporous Mater.* **1995**, *5*, 143.
(8) Mel'nichenko, Y. B.; Schüller, J.; Richert, R.; Ewen, B.; Loong, C.-K. *J. Chem. Phys.* **1995**, *103*, 2016.
(9) Edgar, M.; Schubert, M.; Limbach, H. H.; Göltner, C. G. *Ber. Bunsen−Ges. Phys. Chem.* **1997**, *101*, 1769.
(10) Gjerdaker, L.; Sorland, G. H.; Aknes, D. W. *Microporous Mesoporous Mater.* **1999**, *32*, 305.
(11) Jobic, H. *Phys. Chem. Chem. Phys.* **1999**, *1*, 525.
(12) Ladizhansky, V.; Hodes, G.; Vega, S. *J. Phys. Chem. B* **2000**, *104*, 1939.
(13) Aknes, D. W.; Gjerdaker, L. *J. Mol. Struct. (THEOCHEM)* **1999**, 27.
(14) Courivaud, F.; Hansen, E. W.; Kolboe, S.; Karlsson, A.; Stöcker, M. *Microporous Mesoporous Mater.* **2000**, *37*, 223.
(15) Kitaigorodski, A. I. *Molekülkristalle*; Akademie−Verlag: Berlin, 1979.
(16) Kimmich, R.; Weber, H. W. *Phys. Rev. B* **1993**, *47*, 788.
(17) Kimmich, R.; Klammler, F.; Skirda, V. D.; Serebrennikova, I. A.; Maklakhov, A. I.; Fatkullin, N. *Appl. Magn. Reson.* **1993**, *4*, 425.
(18) Kimmich, R. *NMR Tomography Diffusometry Relaxometry*; Springer: Berlin, 1997.
(19) Bodurka, J.; Gutsze, A.; Buntkowsky, G.; Limbach, H.-H. *Z. Chem. Phys.* **1995**, *190*, 99.
(20) Bodurka, J.; Buntkowsky, G.; Gutsze, A.; Limbach, H.-H. *Z. Naturforsch., C: Biosci.* **1996**, *51C*, 81.
(21) Bodurka, J.; Buntkowsky, G.; Gutsze, A.; Limbach, H.-H. *Appl. Spectrosc.* **1996**, *50*, 1421.
(22) Gutsze, A.; Bodurka, J.; Olechnowicz, R.; Buntkowsky, G.; Limbach, H.-H. *Z. Naturforsch., C: Biosci.* **1995**, *50C*, 410.
(23) Jansen-Glaw, B.; Roessler, E.; Taupitz, M.; Vieth, H. M. *J. Chem. Phys.* **1989**, *90*, 6858.
(24) Börner, K.; Diezemann, G.; Roessler, E.; Vieth, H. M. *Chem. Phys. Lett.* **1991**, *181*, 563.
(25) Roessler, E.; Taupitz, M.; Vieth, H. M. *J. Phys. Chem.* **1990**, *94*, 6879.
(26) Roessler, E.; Taupitz, M.; Börner, K.; Schulz, M.; Vieth, H. M. *J. Chem. Phys.* **1990**, *92*, 5847.
(27) Schmidt-Winkel, P.; Lukens, W. W.; Zhao, D.; Yang, P.; Chmelka, B. F.; Stucky, G. D. *J. Am. Chem. Soc.* **1999**, *121*, 254.
(28) Lettow, J. S.; Han, Y. J.; Schmidt-Winkel, P.; Yang, P.; Zhao, D.; Stucky, G. D.; Ying, J. Y. *Langmuir* **2000**, *16*, 8291.
(29) Schmidt-Winkel, P.; Lukens, W. W.; Yang, P.; Margolese, D. I.; Lettow, J. S.; Ying, J. Y.; Stucky, G. D. *Chem. Mater.* **2000**, *12*, 686.
(30) Ok, J. H.; Vold, R. R.; Vold, R. L.; Etter, M. C. *J. Phys. Chem.* **1989**, *93*, 7618.
(31) Schulz, M.; van der Est, A.; Roessler, E.; Kossmehl, G.; Vieth, H. M. *Macromolecules* **1991**, *24*, 5040.
(32) Geil, B.; Isfort, O.; Boddenberg, B.; Favre, D. E.; Chmelka, B. F.; Fujara, F. *J. Chem. Phys.* **2002**, *116*, 2184.
(33) Boddenberg, B.; Grosse, R. *Z. Naturforsch., A: Phys., Phys. Chem., Kosmophys.* **1986**, *41A*, 1361.
(34) Xion, J.; Maciel, G. E. *J. Phys. Chem. B* **1999**, *103*, 5543.
(35) Slichter, C. P. *Principles of Magnetic Resonance*, 3rd ed.; Springer−Verlag: Berlin, Heidelberg, New York, 1990.
(36) Schmidt-Rohr, K.; Spiess, H. W. *Multidimensional Solid State NMR and Polymers*; Academic Press: London, 1994.
(37) Schreiber, A. Phasenverhalten reiner Stoffe in mesoporösen Silika-Materialien. Ph.D. Thesis, Technische Universität Berlin, Germany, 2002.
(38) Dollimore, D.; Heal, G. R. *J. Appl. Chem.* **1964**, *14*, 109.
(39) Brunauer, S.; Emmett, P. H.; Teller, E. *J. Am. Chem. Soc.* **1938**, *60*, 309.
(40) Barrett, E. P.; Joyner, L. G.; Halenda, P. P. *J. Am. Chem. Soc.* **1951**, *73*, 373.
(41) Buntkowsky, G.; Sack, I.; Limbach, H.-H.; Kling, B.; Fuhrhop, J. *J. Phys. Chem. B* **1997**, *101*, 11265.
(42) Wehrmann, F.; Fong, T.; Morris, R. H.; Limbach, H.-H.; Buntkowsky, G. *Phys. Chem. Chem. Phys.* **1999**, *1*, 4033.
(43) Gedat, E.; Schreiber, A.; Albrecht, J.; Shenderovich, I.; Findenegg, G.; Limbach, H.-H.; Buntkowsky, G. *J. Phys. Chem. B* **2002**, *106*, 1977.
(44) Mehring, M. *High-Resolution NMR Spectroscopy in Solids*; Springer−Verlag: Berlin, Heidelberg, New York, 1983.
(45) Zaremba, S. K. *Ann. Mater. Pure. Appl.* **1966**, *4*, 293.
(46) Conroy, H. *J. Chem. Phys.* **1967**, *47*, 5307.
(47) Cheng, V. B.; Suzukawa, H. H.; Wolfsberg, M. *J. Chem. Phys.* **1973**, *59*, 3992.
(48) Spiess, H. W.; Sillescu, H. *J. Magn. Reson.* **1981**, *42*, 381.
(49) Cox, E. G.; Cruickshank, D. W. J.; Smith, J. A. S. *Proc. R. Soc. London, Ser. A* **1958**, *247*, 1.
(50) Shenderovich, I.; Buntkowsky, G.; Schreiber, A.; Gedat, E.; Sharif, S.; Albrecht, J.; Golubev, N. S.; Findenegg, G. H.; Limbach, H. H. *J. Phys. Chem. B* **2003**, *107*, 11924.
(51) Grünberg, B.; Emmler, T.; Gedat, E.; Shenderovich, I.; Findenegg, G. H.; Limbach, H. H.; Buntkowsky, G. *Chemistry Eur. J.* **2004**, *10*, 5689.